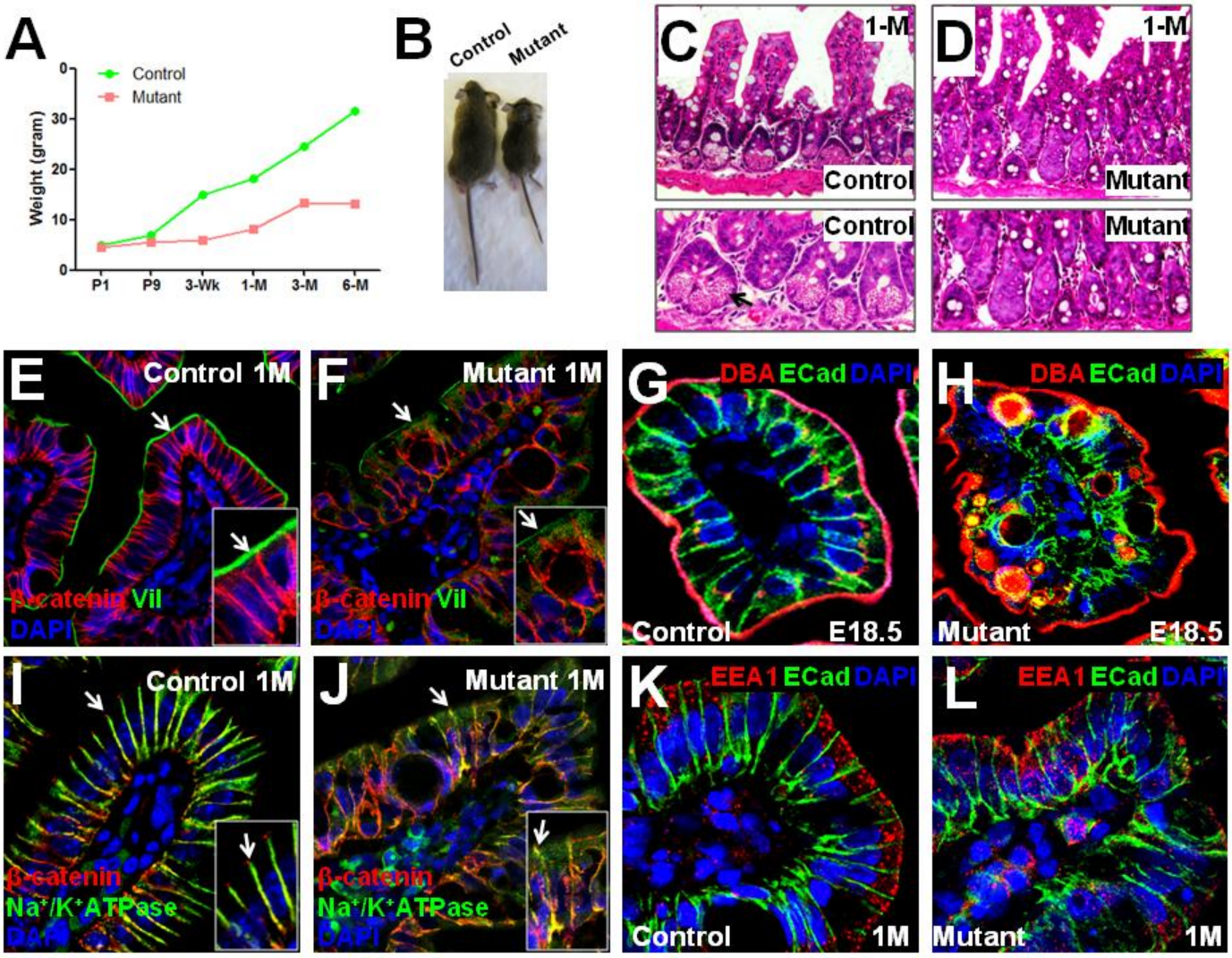

Supplementary Figure 1. Growth retardation and intestinal abnormality in *Cdc42$^{loxP/loxP}$;VillinCre* mice.
(A) Growth curves of control and Cdc42 mutant mice. (B) P15 control and mutant littermates. (C-D) H&E staining for one-month control and Cdc42 mutant jejunum. Arrow in lower panel of C points to the typical Paneth cell granules present in control crypt. (E-F) Villin and E-cadherin staining of control and mutant jejunum. Arrows indicate brush borders. (G-H) DBA lectin and E-cadherin staining of control and mutant jejunum. (I-J) Na^+/K^+-ATPase and β-catenin staining of control and mutant jejunum. Arrows indicate tight junctions. (K-L) EEA1 and E-cadherin staining of control and mutant jejunum.

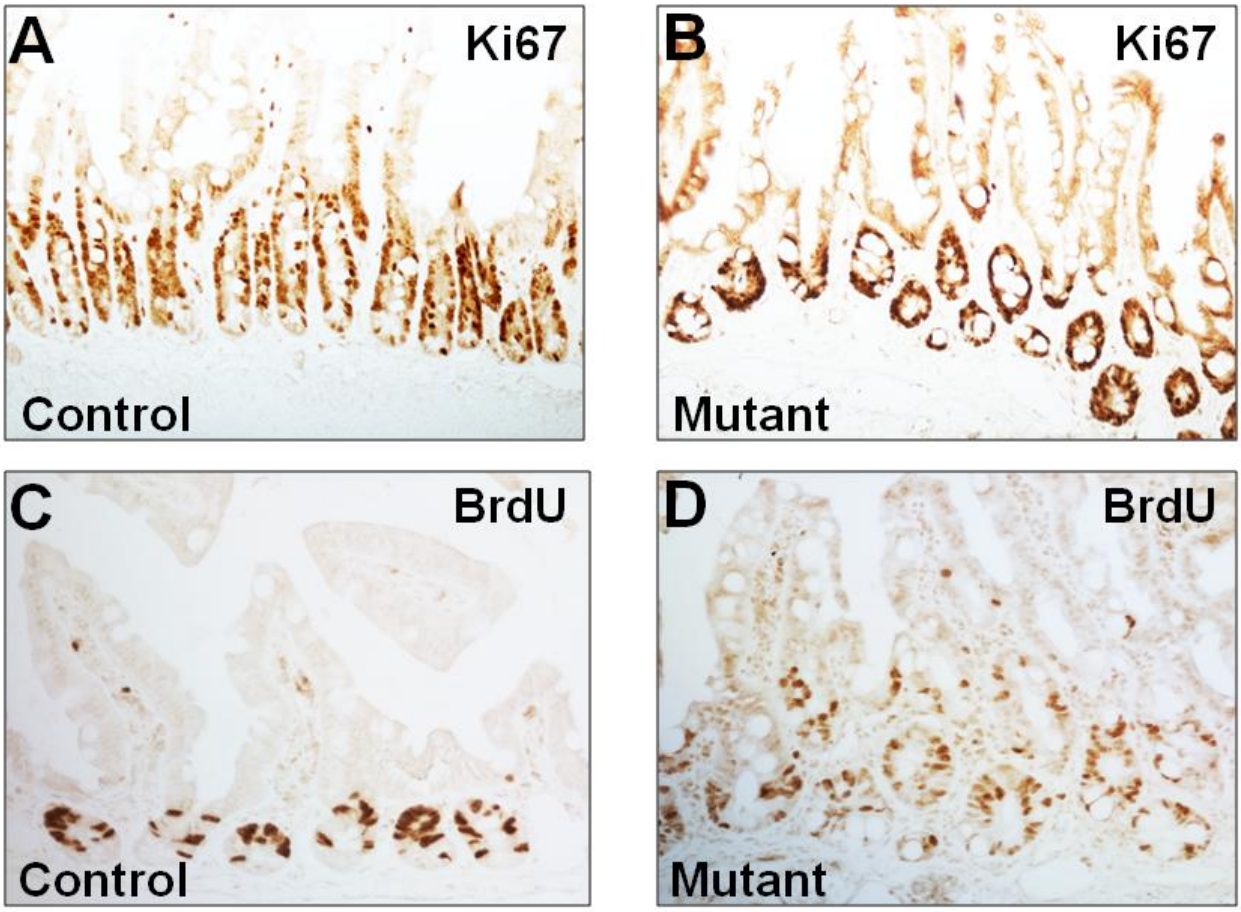

Supplementary Figure 2. Affected stem/progenitor cell proliferation in Cdc42-mutant intestines.

(A-B) Ki67 staining. (C-D) BrdU staining.

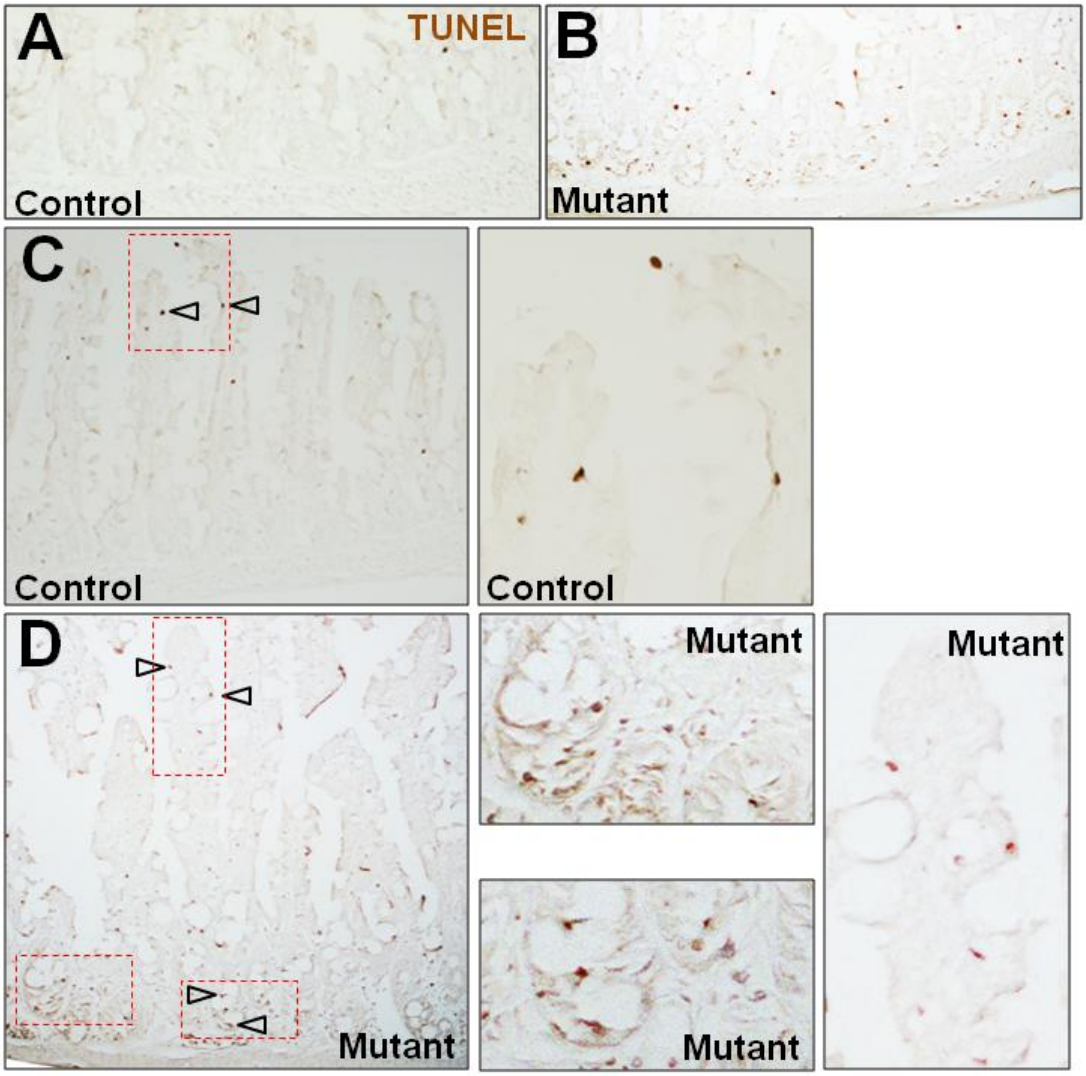

Supplementary Figure 3. Increased apoptosis in Cdc42 mutant intestinal crypts.

(A-D) TUNEL staining. Arrowheads point to apoptotic cells in control villus tips in C, and mutant crypts and villi in D.

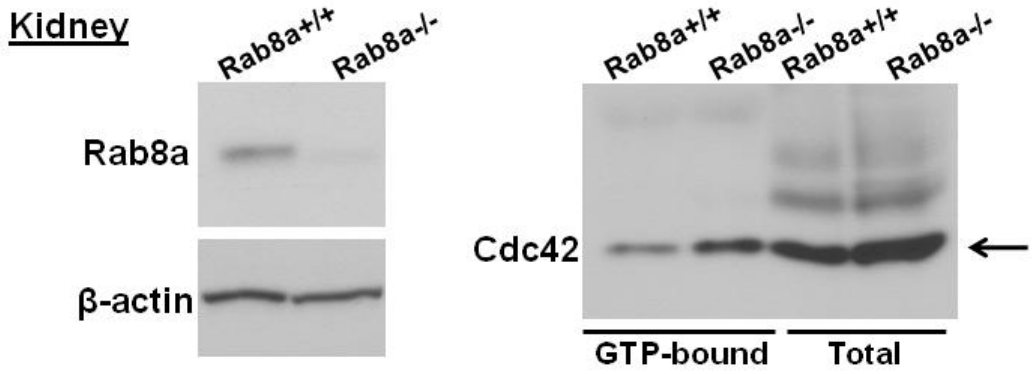

Supplementary Figure 4. Cdc42-GTP activity is not changed in Rab8a knockout kidney.

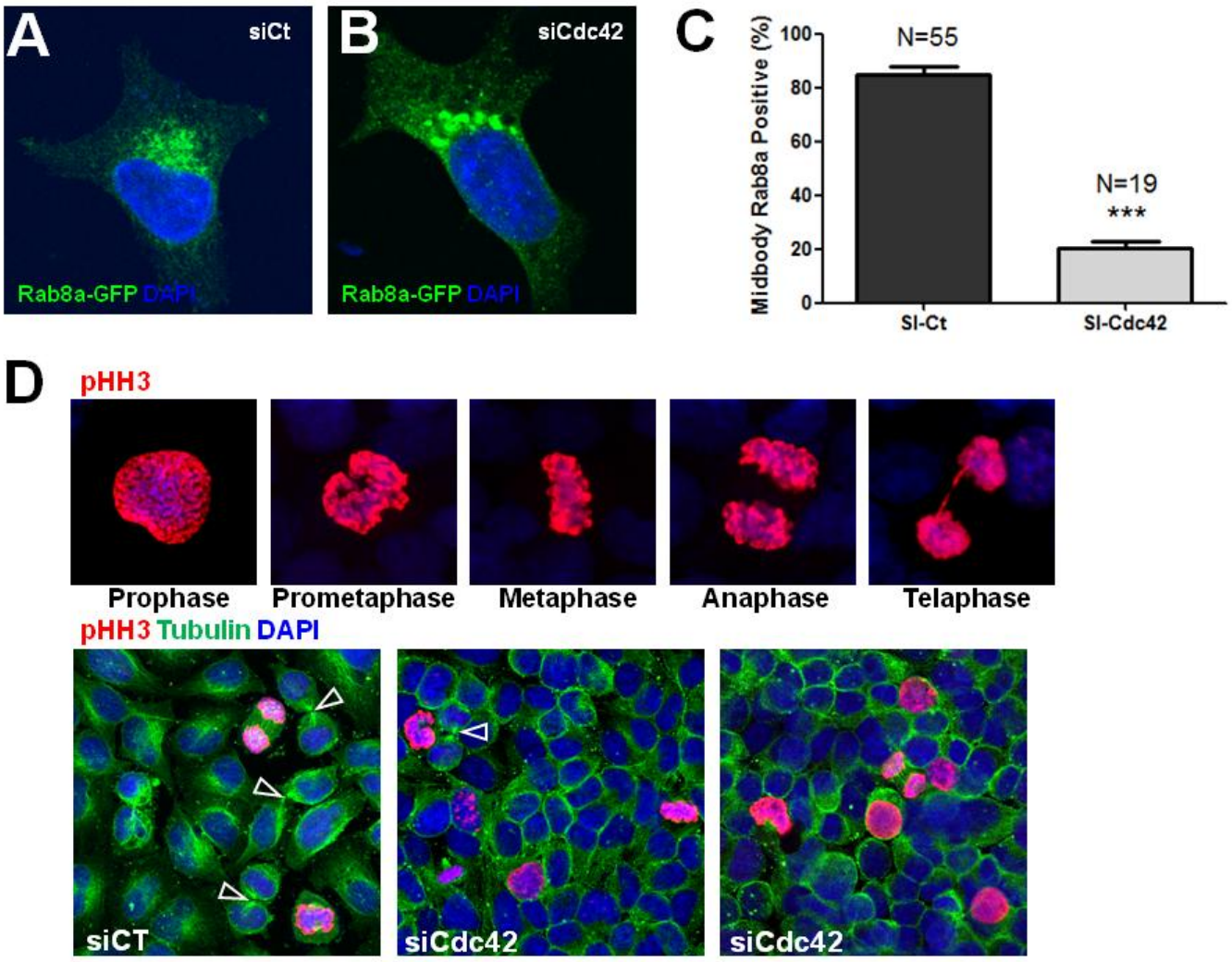

Supplementary Figure 5. Cdc42-deficiency affects midbody-trafficking of Rab8a vesicles, impeding cytokinesis.

(A-B) Rab8a-GFP distribution in live control and Cdc42 knockdown cells at interphase. (C) Quantification of Rab8a-GFP positive at midbody from three independent experiments. (D) pHH3 and Tubulin staining identify mitotic and cytokinetic events in control and Cdc42 knockdown cells.

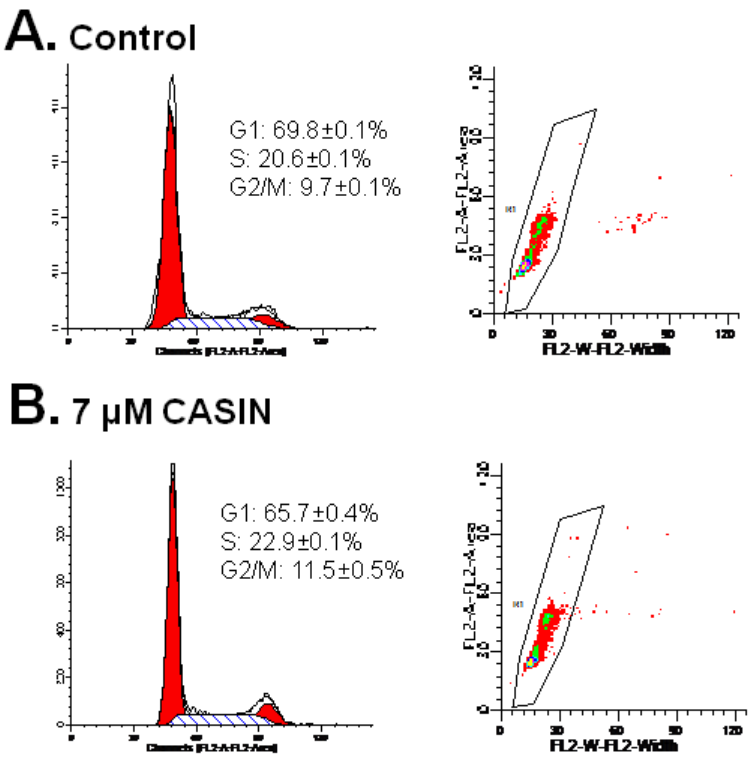

Supplementary Figure 6. CASIN inhibition of Cdc42 induces G2/M accumulation.

(A-B) FACS cell cycle analysis of control and 7 µM CASIN treated cells.

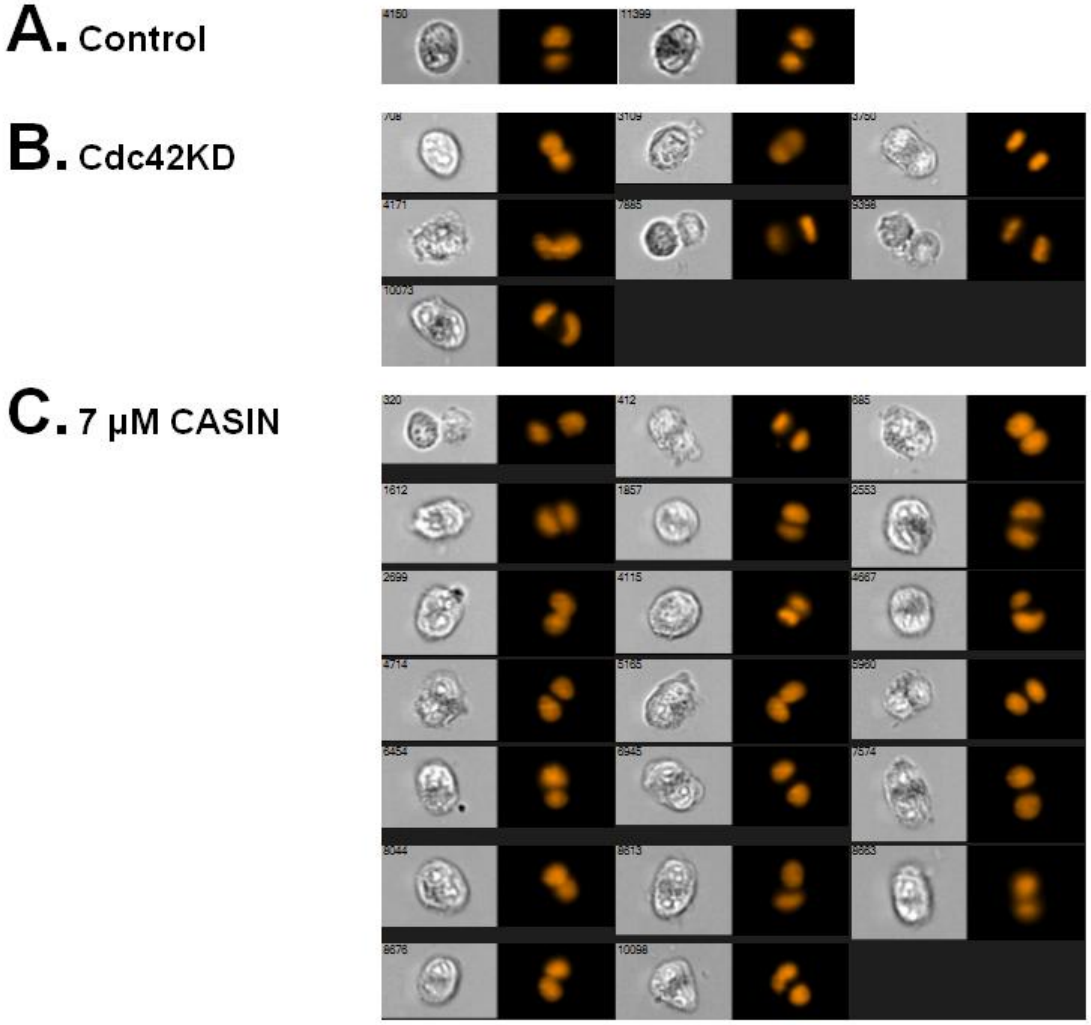

Supplementary Figure 7. Cdc42 inhibition causes accumulation of cells at anaphase.

(A-C) Imaging Flow Cytometry demonstrates increased anaphase counts in Cdc42 knockdown and 7 µM CASIN treated cells.

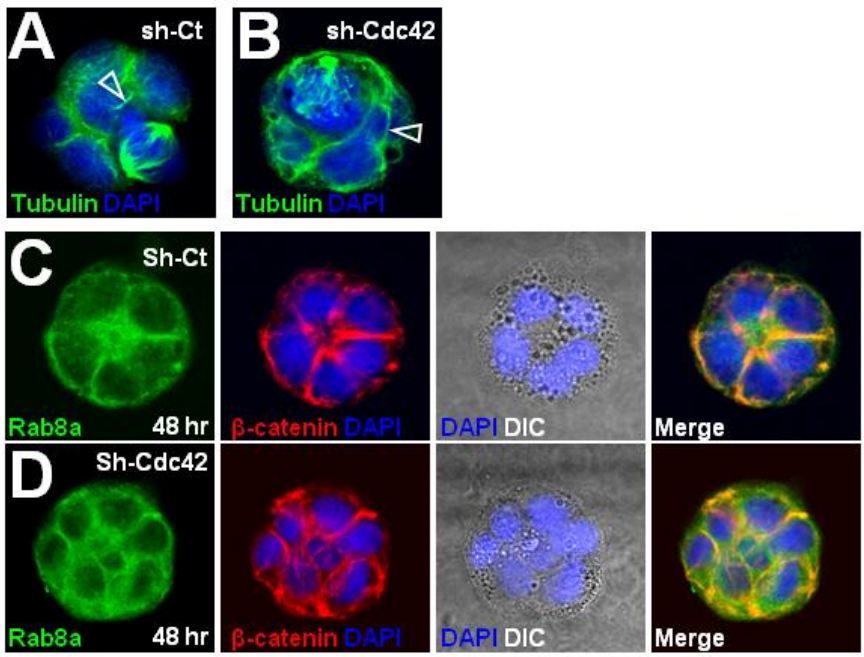

Supplementary Figure 8. Cdc42-depletion disrupts Rab8a-vesicle traffic, midbody orientation and epithelial morphogenesis.

(A-B) Tubulin staining in control and Cdc42-depleted Caco2 cysts. Arrowheads point to midbodies. Note that control midbody is positioned towards lumen. (C-D) Rab8a and β-catenin staining of control and Cdc42-depleted Caco2 cysts.

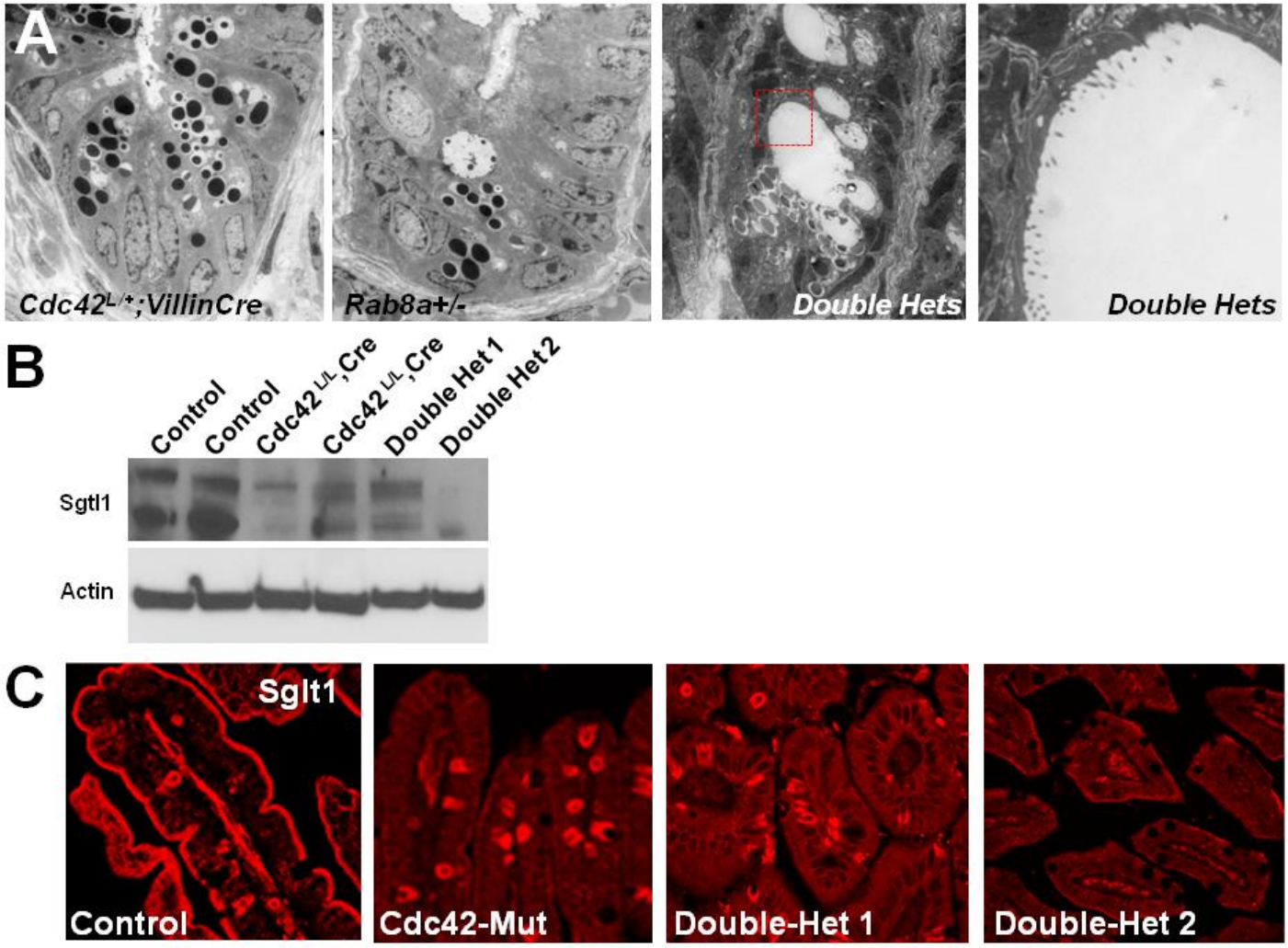

Supplementary Figure 9. Cdc42 and Rab8a double heterozygous intestines show abnormal crypt morphology and Sglt1 localization.

(A) TEM graphs of control and double heterozygous mouse intestinal crypts. (B) Western blots for Sgtl1. (C) Sglt1 immunofluorescent staining in control, Cdc42 mutant and double heterozygous mice. From B and C, please note that variability exists between different animals indicating a different disease penetrance.

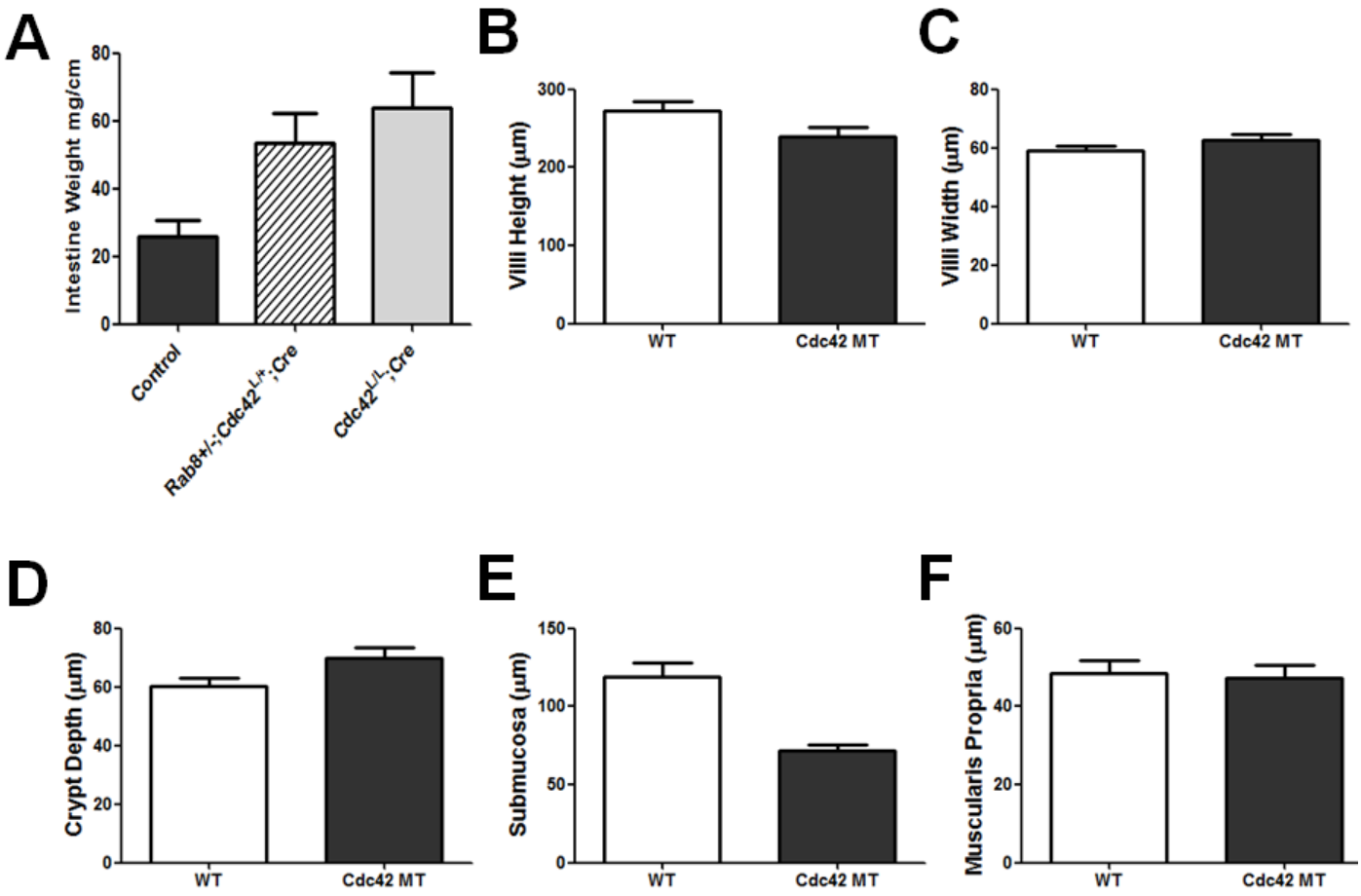

Supplementary Figure 10. Cdc42 mutant and double heterozygous mice show increased intestinal weights indicating tissue edema.

(A) Intestinal weight per surface area. (B-F) Morphometric analyses of intestinal villi height, width, crypt depth, submucosa and muscle thickness.

Supplementary Table 1: Primer sequences for RT-PCR analyses.

		Primer Sequence
Lgr5	F	TAAAGACGACGGCAACAGTG
	R	GCCTTCAGGTCTTCCTCAAA
Olfm4	F	TGAAGGAGATGCAAAAACTGG
	R	CTCCAGCTTCTCTACCAAGAGG
Bmi1	F	GAGCAGATTGGATCGGAAAG
	R	GCATCACAGTCATTGCTGCT
Msi1	F	ACTCCGGGGTCAGCAGTTAC
	R	GTGGTACCCATTGGTGAAGG
Hopx	F	AGCAGACGCAGAAATGGTTT
	R	TGGCTCCCTAGTCCGTAACA
Defa5	F	TATCTCCTTTGGAGGCCAAG
	R	TTTCTGCAGGTCCCAAAAAC
Lyz	F	TCAGATCAATAGCCGATACTGG
	R	ATTGTATGGCTGCAGTGATGTC
Mmp7	F	CTTACAAAGGACGACATTGCAG
	R	AGTGCAGACCGTTTCTGTGAT
Pla2v5	F	AACTGGAGGAAAAAGACTGTGC
	R	ATTGGACAGAAGGAGTCGTGTT